epl A Letters Journal Exploring the Frontiers of Physics

July 2018

EPL, **123** (2018) 14003 www.epljournal.org
doi: 10.1209/0295-5075/123/14003

Threshold of gas-like to clustering transition in driven granular media in low-gravity environment

M. Noirhomme[1(a)], A. Cazaubiel[2], A. Darras[1], E. Falcon[2], D. Fischer[3], Y. Garrabos[4], C. Lecoutre-Chabot[4], S. Merminod[2], E. Opsomer[1], F. Palencia[4], J. Schockmel[1], R. Stannarius[3] and N. Vandewalle[1]

[1] *Group for Research and Applications in Statistical Physics (GRASP), CESAM Research Unit, Physics Department, B5a, University of Liège - B-4000 Liège, Belgium*
[2] *Université Paris Diderot, Sorbonne Paris Cité, MSC, UMR 7057 CNRS - F-75013 Paris, France*
[3] *Institute of Physics, Otto von Guericke University - D-39106 Magdeburg, Germany*
[4] *Institut de Chimie et de la Matière Condensée de Bordeaux (ICMCB)-UPR 9048 CNRS F-33608 Pessac, France*

received 30 May 2018; accepted in final form 17 July 2018
published online 13 August 2018

PACS 45.70.-n – Granular systems
PACS 45.70.Qj – Pattern formation

Abstract – Strongly driven granular media are known to undergo a transition from a gas-like to a cluster regime when the density of particles is increased. However, the main mechanism triggering this transition is not fully understood so far. Here, we investigate experimentally this transition within a 3D cell filled with beads that are driven by two face-to-face vibrating pistons in low gravity during parabolic flight campaigns. By varying large ranges of parameters, we obtain the full phase diagram of the dynamical regimes reached by the out-of-equilibrium system: gas, cluster or bouncing aggregate. The images of the cell recorded by two perpendicular cameras are processed to obtain the profiles of particle density along the vibration axis of the cell. A statistical test is then performed on these distributions to determinate which regime is reached by the system. The experimental results are found in very good agreement with theoretical models for the gas-cluster transition and for the emergence of the bouncing state. The transition is shown to occur when the typical propagation time needed to transmit the kinetic energy from one piston to the other is of the order of the relaxation time due to dissipative collisions.

Copyright © EPLA, 2018

Introduction. – When submitted to an external energy input, confined granular matter exhibits different dynamics depending on the filling and forcing conditions of the system [1]. These different dynamical regimes can be classified into three categories called "solid" [2–4], "liquid" [5] or "gas", in analogy to the classical counterpart. This letter is focused on very dilute systems with strong enough forcing, where particles can move erratically and have a gas-like behavior. However, such a granular gas displays properties strikingly different from those of a molecular gas: anomalous scalings of pressure [6] and collision frequency [7], and non-Gaussian distribution of particle velocity [8]. These differences are mainly attributed to the dissipation occurring during inelastic collisions between particles. Continuous injection of energy is thus necessary to sustain a stationary state in this dissipative out-of-equilibrium system. This is usually performed experimentally by vibrating a container wall or the whole container. When the forcing is stopped, numerical simulations have shown the formation of density gradients during the cooling (instability of the homogeneous cooling state) [9] as well as inelastic collapse (particles undergoing an infinite number of collisions in finite time) [10]. The predicted duration of the cooling phase [11] has been tested experimentally with success [12]. Due to the dissipative character of the collisions, increasing the density within a driven granular gas, and thus the number of collisions, will lead to an increase of the energy dissipation in the system. A cluster formation can then occur at high enough density despite the continuous energy injection. Such a transition from a gaseous regime to a cluster of particles when the density increases has been

(a) E-mail: mnoirhomme@uliege.be

established almost 20 years ago [6,13,14]. The parameters triggering this transition are far from being fully understood even though this observation has been reproduced numerically [15].

On Earth, experiments are biased by gravity-induced anisotropy and by the friction forces that act on all the particles composing the system. Low-gravity environment is thus needed for granular gases in order to obtain an experimental situation for which inelastic collisions are the only interaction mechanism between particles. For instance, the cluster formation was first observed experimentally on Earth in 3D [6] and 2D [13], and has then been more clearly demonstrated in low gravity in 3D [14]. More recently, a Topical Team of the European Space Agency (ESA) has designed an instrument called VIP-Gran (for Vibrated Induced Phenomena in Granular matter) [16]. It aims to study the dynamics and statistical mechanics of driven granular systems in low-gravity environment from dilute to dense regimes [17].

In this work, we study experimentally the transition from a granular gas to a clustered state in low gravity using the 3D VIP-Gran facility. The full experimental phase diagram is then obtained for large ranges of experimental parameters. These results are compared with numerical and theoretical work predicting the marginal curve of the phase diagram separating the gas- and liquid-like regimes [18]. Good agreement is found during this comparison showing that this transition is governed by the interplay between inertia (propagation time between collisions) and inelasticity (relaxation time due to dissipative collisions). This work follows the footsteps of Sack *et al.* [19] and Falcon *et al.* [14] where the authors have observed similar granular states in different geometries and for different excitations.

Setup. – The setup of the VIP-Gran instrument has been extensively described in [17]. We only recall here its main features regarding the experiments discussed in this work. As sketched in fig. 1, it consists of a cell of dimension $60 \times 30 \times 30$ mm where the energy is injected into the system by two oscillating pistons, separated by an average distance L. The latter can be tuned to control the accessible volume of the cell. The two opposite pistons, moved by linear voice-coil motors, are driven sinusoidally in phase opposition with the same frequency f and amplitude A. The vibration axis is perpendicular to the moving walls (see fig. 1). The cell is filled with N bronze beads of diameter $d = 1$ mm, either manually or automatically using a bead-feeding device [17]. Experimental data are acquired using two high-speed cameras of maximal frame rates $f_c = 1000$ fps with a resolution of 1024×900 pixels. Visualizations of the cell are obtained in the two directions perpendicular to the vibration axis (see fig. 1). During one period of vibration $T = 1/f$ (with a frequency f at most equal to 20 Hz), the number of recorded images is $f_c T$, that is 50 images at least. The control parameters are the number of beads N, the mean distance L between vibrating

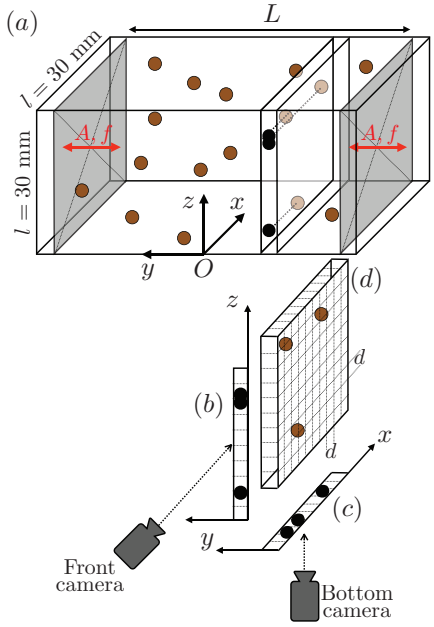

Fig. 1: (Color online) (a) Sketch of the experimental VIP-Gran cell. The oscillating pistons are colored in light grey. The recorded images of the cell are numerically divided in slices of width d along the y-axis (axis of vibration). Front (b), bottom (c) and side (d) views of the slice are sketched. The front and bottom views are the two accessible shadow profiles while the side view is an arbitrary distribution which could have generated these observations. The link between the measured shadow and the possible number of particles in the slices is explained in the main text. (d) Each slice is divided into rows and columns of dimension d into the x and z directions.

pistons, the amplitude A and frequency f of the forcing. The distance between the walls oscillates as a consequence between $L - 2A$ and $L + 2A$. The packing fraction is then defined as $\Phi = N\mathcal{V}_g/V$, where $\mathcal{V}_g = \pi d^3/6$ is the volume of a single grain, $V = l^2(L + 2A)$ the maximum cell volume, and $l = 30$ mm. We focus here on dilute regimes with $\Phi < 10\%$. All relevant experimental parameters are listed in table 1. The filling parameters were chosen according to numerical simulations predicting the transition from a gaseous state to a clustered state in the VIP-Gran cell [18]. Moreover, since these simulations do not predict a qualitative change with vibration frequency [20], f will not be varied systematically here. To cover the whole ranges of experimental parameters, five ESA Parabolic Flight Campaigns (PFCs #63 to 67) were performed on board of a specially modified Airbus A310 Zero-G aircraft of Novespace through a series of parabolic trajectories which result in low-gravity periods, each of approximatively 22 s. Low-gravity environment is about $\pm 0.05g$. Each PFC lasts 3 days with 31 low-gravity parabolae per day. Among the 465 parabolae performed, 114 were dedicated to the present study.

Results. – The raw data of the experiments consist of two sequences of greyscale pictures of the cell, taken

Table 1: Parameters of each experiment performed during ESA parabolic flight campaigns #63 to 67. Each set of parameters was precisely chosen in order to reach different regimes of the phase diagram displayed in fig. 3.

PFC	#runs	L(mm)	A(mm)	f(Hz)	N	Symbol
63	25	40.0	[1.0; 1.4; 1.8; 2.0; 2.5]	20	[250; 750; 1250; 1750; 2750]	□
64	15	[12.5; 20.0; 27.5]	[0.5; 1.0; 1.5; 2.0; 2.5]	20	[1611; 2578; 3545]	△
65	15	[30.0; 35.0; 40.0]	[2.0; 2.5; 3.0; 3.5; 4.0]	15	[2578; 3008; 3438]	◇
66	12	40.0	[4.0; 5.0]	15	[2578; 3438; 4297; 5157; 6016; 6875]	○
67	30	[20.0; 25.0; 30.0; 35.0; 40.0]	3.0	15	[250; 500; 1000; 1500; 2000; 2500]	⬠

by both high-speed cameras. About 40000 images are recorded for one single parabola, and of the order of 4.5 millions for all parabolae. As displayed in fig. 2, three typical dynamical granular regimes are observed in our experiment depending on the number N of particles in the cell. A granular gas regime is observed for very dilute densities (fig. 2(a)) where particles are homogeneously distributed within the entire cell. When the density is increased, we observe a cluster of particles almost static in the middle of the cell, the cluster being surrounded by lower particle density regions (see fig. 2(b)). In these regions, the particles have fast velocities and transmit the kinetic energy from the pistons to the cluster where it is mainly dissipated. The third observed regime consists in a cluster of all particles that bounces periodically from one piston to the other one (fig. 2(c)), as previously observed [21]. We called this regime afterwards "bouncing aggregate". The period of oscillation of the latter is subharmonics, *i.e.*, twice the piston period. This regime occurs when the vibration amplitude exceeds a critical fraction of the cell size (see below). For the corresponding time evolutions, see supplementary slow-down videos `gas.mp4`, `cluster.mp4` and `bouncing.mp4`. By using image processing tools, we will now infer from these images the spatial density profiles for these three regimes.

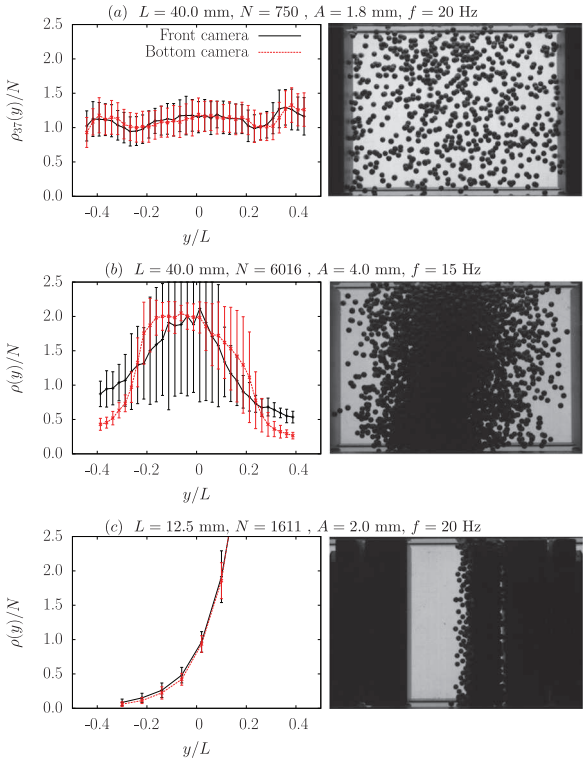

Fig. 2: (Color online) Right: different dynamical regimes for different experimental parameters L, N, A, and f: granular gas (a), cluster (b), and bouncing aggregate (c). The picture come from the front camera. Left: corresponding average density profiles $\rho(y)$ of the system obtained from the image processing (see text). The red (respectively, black) curves are inferred from images from the bottom (respectively, front) camera. For the granular gases and the clusters, the average density profiles are very stable over time. It is not the case for the bouncing aggregate for which the position of the peak in the average density profile varies over time.

Image processing. – For each low-gravity phase, we wait a few seconds ($50T$) before recording data, in order to reach a stationary state within the granular medium. From there on, data is recorded during $100T$ (between 5 and 7 s). This corresponds to the middle of the parabola duration, when the fluctuations of gravity, called g-jitters, are the weakest. In order to obtain some quantitative data from the pictures, we performed image analysis using the open-access software FIJI [22]. First, we applied a threshold on the pictures, coloring each pixel either black (corresponding to the shadow coming from the presence of one or more grains) or white (reporting no particle between the light and the camera), depending on their grey level. The second step consists in dividing the constant free zone of the system into slices along the vibration axis (y-axis) (see fig. 1). Each slice has a width d, the particle diameter, and is located at the dimensionless position $y \in [(-L/2 + A)/Ld; (L/2 - A)/Ld]$.

The aim of the image processing described in this section is to reconstruct the average 3D density profile of the system using the 2D pictures. In the following, the processing will be detailed only for the bottom camera images, *i.e.*, in the (x, y)-direction. The processing in the other direction is exactly the same. First, we divided the considered slice into columns of width d. This implies a division of the (x, y)-plane in squares of area d^2. An example of the division of a slice is given in fig. 1. By assuming a uniform distribution of the grains in the slice, the probability of the presence of one of those grains in a specific

column is $p = d/l$. If the slice contains N_y particles, the probability $P(X = n)$ of finding n grains in the column is given by the binomial distribution

$$P(X = n) = \binom{N_y}{n} p^n (1-p)^{N_y - n}, \tag{1}$$

where X is the random variable representing the number of grains in a column, and $\binom{N_y}{n} = N_y!/[n!(N_y - n)!]$ the binomial coefficient. By equaling $X = 0$ (*i.e.*, by focusing on the light transmitted through the system), the number of particles in the slice can be isolated. One obtains

$$N_y = \frac{\ln(1 - s_x)}{\ln(1 - d/l)}, \tag{2}$$

where s_x, the shadow density measured by the bottom camera, is given by the number of black pixels in the (x, y)-plane divided by the total number of pixels in the surface ld. See the supplementary material `Supplementarymaterial.pdf` for more details.

Note again that the main hypothesis is that the particles are uniformly distributed in each slice. This assumption seems reasonable if there is no external residual acceleration in the system. In addition, note that the number N_y of particles in a slice is undetermined, from eq. (2), for $s_x = 1$. This extreme value is mostly unreached, except for a few pictures given by the bottom camera, for parabolae where the g-jitters were significant. In these cases, the maximal number of grains in the considered slice was fixed at 300. This value corresponds to the detection of a single white pixel in s_x. Finally, the normalized distribution of the number of grains in the slices N_y/N as a function of y can be found for each image provided by the cameras. We have averaged the distributions coming from all the pictures determined by a fixed piston phase in order to obtain f_c/f different distributions.

Statistical analysis. – The average density profiles of the system are shown in fig. 2, for different parabolae (corresponding to different parameters listed in table 1). For the gaseous state, the distribution is approximatively uniform (see fig. 2(a)). By contrast, when a clustered state is reached, the resulting distribution exhibits systematically a peak. If the cluster is stabilized in the middle of the cell, the position of the resulting peak in the distribution is stable over the time, too (see fig. 2(b)). However, in the case of the bouncing aggregate, the bulk moves from one piston to the other one. Consequently, the position of the resulting measured peak varies over the time (see fig. 2(c)). Note that we found nearly always differences between the distributions obtained from the two different cameras. Actually, the g-jitters tend to gather the grains close to the bottom of the cell, making the z-distribution more uniform than the x-distribution over the y-axis. In the cluster regime, the error bars in the distributions are also larger for the z-distribution than for the x one, due to prevailing g-jitters in the z-direction.

In order to extract the state of the system from the averaged distributions coming out of our image processing, we use the one-sample Kolmogorov-Smirnov (KS) test [15,18]. This KS test consists in comparing the measured cumulated distributions with a theoretical one. In analogy with classical gases, we assume that a granular gas is characterized by a uniform distribution of the position of the particles in the cell. In the KS test, the comparison between two distributions is performed by measuring the maximal distance separating the measured cumulated distribution, noted $F(y)$, computed using the corresponding average density profile $\rho(y)/N$, and the theoretical cumulated distribution, noted $U(y)$. This distance is defined as

$$D = \sup_{|y| \leq L/2 - A} |F(y) - U(y)|\cdot \tag{3}$$

Then, we compared D to a given threshold-value K_α coupled to the number of classes characterizing the distributions, noted k. Following our division of the cell into slices, this number of classes is simply given by $k = L/d$. Concerning the threshold K_α, its value depends on the level of significance of the test, α, which has been fixed at 0.01 in order to follow previous works [15,18]. The KS test of eq. (2) allows us to consider that the system has reached a clustered state as soon as the condition $D > K_\alpha/\sqrt{k}$ is fulfilled. On the other hand, as long as the threshold is not crossed, the grains can be considered as uniformly distributed in the cell and the system is considered in a gaseous phase. We applied the KS test on each averaged distribution $F(y)$ (corresponding to each different piston phase) obtained from the image processing. We found two final averaged values of the maximal distances D_x and D_z for all averaged distributions $F(y)$ coming from each camera. These values D_x and D_z are two statistical characterizations of the averaged distribution of the position of the particles along the vibration axis for a given set of parameters. For each parabola of each PFC, we calculated D_x and D_z and compared the obtained values to the related threshold. The state of the system can be deduced from D_x and D_z. We detected a gaseous regime (see the red symbols in the phase diagram of fig. 3) if the conditions $D_x \leq K_\alpha/\sqrt{k}$ and $D_z \leq K_\alpha/\sqrt{k}$ are fulfilled. Otherwise, the system is considered as clustered (see the green symbols in fig. 3). We reported these comparisons in the phase diagram shown in fig. 3.

Phase diagram. – In fig. 3, we plot the typical length scale of the system δ, normalized by the particle radius, R, as a function of the packing fraction ϕ. More precisely, δ is the mean distance that N particles achieve when they pass across a constraint free distance $(L-2A)$. This mean value is numerically calculated and is tabulated as a function of the chosen experimental parameter set (L and A) [18]. The horizontal axis reports the mean packing fraction of the system,

$$\Phi = N \frac{4\pi R^3}{3(L + 2A)l^2}\cdot$$

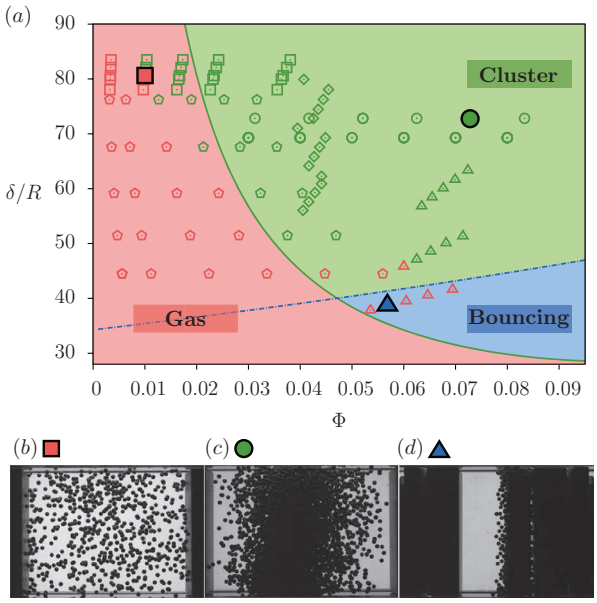

Fig. 3: (Color online) (a) Phase diagram of the dynamical regimes, observed in the PFC experiments, as a function of the dimensionless system size, δ/R, and the packing fraction, ϕ. The experimental parameters and corresponding symbols are listed in table 1. Granular gas (red), cluster (green), and bouncing (blue) regimes are detected with a statistical test (see text). The theoretical solid line is from eq. (4) with $C_0 = 1$, $R_0 = 2$, and $\epsilon = 0.9$. The dashed line corresponds to the right-hand term of eq. (5). Bottom: typical front views of the cell showing gas (b), cluster (c) and bouncing (d) regimes corresponding to the plain symbols in (a).

The instrument geometry limits the accessible region of the phase diagram to $30 < \delta/R < 90$. All experiments performed during PFCs are represented by symbols which correspond to sets of parameters listed in table 1. The solid curve plotted in the phase diagram is the theoretical frontier separating the gaseous regime from the cluster one. This marginal curve comes from a theoretical model comparing the decay time of energy in the system (Haff time [11]) and the time needed for a particle to cross the whole cell in response to an energy impulse coming from the pistons (propagation time), that is [18]

$$\frac{\delta}{R} = \frac{1}{3\Phi} \frac{\ln\left[1 + \frac{C_0}{\varepsilon(1+\varepsilon)(1-3R_0\Phi)}\right]}{\ln\left(1/\varepsilon\right)}, \qquad (4)$$

where ε is the restitution coefficient of the particles and C_0 and R_0 are two adjustable parameters whose values have been evaluated with the help of numerical simulations. The theoretical model of eq. (4) is found to be in good agreement with most experiments (see fig. 3). However, for $\Phi < 3\%$ and $\delta/R \gtrsim 75$, the agreement is not so good (see top left-hand side in fig. 3). This corresponds to experiments performed with a large cell in a diluted regime where the cluster formation is probably induced by g-jitters. Indeed, as soon as a cluster is formed (*e.g.*, by a tiny variation of g), its destruction is very hard to be done since it is located far from the oscillating pistons. The model which considers a uniform distribution of the positions of the particles as initial condition is consequently less adapted in this region of the phase diagram than in others.

The bouncing regime has been only observed for a very narrow cell ($\delta/R \sim 38$, or $L \sim 12.5d$), and has been previously reported numerically for the same configuration as ours [15]. For a configuration where the whole container is vibrated, the condition to observe a bouncing aggregate is predicted theoretically to be $A > (L-e)/\pi$, e being the aggregate thickness [19,21,23]. This means that the cluster center of mass follows the container oscillations when the amplitude of vibration is larger than a fraction of the free space $(L-e)$ between the cluster and the container walls. By adapting this model to our configuration (container walls vibrated in phase opposition), we find that the bouncing regime occurs within a bounded region by the following conditions:

$$\left(\frac{\pi + 2\Phi/\phi_{\mathrm{RLP}}}{1-\Phi/\phi_{\mathrm{RLP}}} - 2\right) < \frac{L}{A} < \left(\frac{2\pi + 2\Phi/\phi_{\mathrm{RLP}}}{1-\Phi/\phi_{\mathrm{RLP}}} - 2\right), \qquad (5)$$

where $\phi_{\mathrm{RLP}} = 0.59$ is the density of a random loose packing pile [24]. Only the upper limit of eq. (5) is visible in fig. 3 (see dashed line separating the cluster region from the bouncing one). Even though the agreement with the single experimental point is good, more experiments are needed to confirm this theory. Finally, note that the analogous of a triple point (δ_t/R, Φ_t) can be defined by the intercept of the two marginal curves within the phase diagram, *i.e.*, by balancing eq. (4) with the right-hand term in eq. (5).

Conclusion. – We have experimentally investigated the gas-like to clustering transition in a driven granular media in 3D low-gravity environment. Experimental parameters have been exhaustively varied (number of particles, cell size, and vibrational parameters). We have observed three dynamical regimes: Granular gas, cluster and bouncing aggregate. These regimes have been characterized by means of two perpendicular cameras leading to the spatial distribution of particles within the cell. We transformed the shadow density measured on each image into profiles of particle density along the vibration axis of the cell. Then, a statistical Kolmogorov-Smirnov test has been performed to compare these experimental distributions with uniform ones in order to deduce the state reached by the system (gas, cluster or bouncing aggregate). The results of these tests were reported in a phase diagram and confronted with theoretical models for the gas-cluster transition and the emergence of the bouncing aggregate. The experimental results are in excellent agreement with the theoretical predictions, except for large and diluted systems where the g-jitters, as small as they can be, have probably a non-negligible impact on the final state of the system. To reach a high level of low-gravity conditions ($\sim 10^{-5} g$) where g-jitters are negligible,

the VIP-Gran instrument is currently in development for the International Space Station. We have thus shown that the gas to clustering transition occurs when the typical propagation time between two collisions is of the order of the relaxation time due to dissipative collisions. This study could lead to applications for space exploration (*e.g.*, handling a granular medium in low gravity by applying vibrations) or to a better understanding of the dynamics of planetary rings in astrophysics.

* * *

We thank M. Braibanti, O. Minster and V. Koehne from ESA for fruitful discussions and for the flight opportunity. VIP-Gran-PF was built by DTM Technologies™ (Modena, Italy). We acknowledge A. Pellegrini, L. Recanatesi, and D. Santachiara from DTM, T. Trittel, University of Madeburg, for technical support, and M. Hou for discussions. We acknowledge the support of Novespace during PFC63 to PFC67, and partial financial support by CNES. This work was funded by ESA Topical Team No. 4000103461.

REFERENCES

[1] de Gennes P. G., *Rev. Mod. Phys.*, **57** (1985) 827.
[2] Liu A. J. and Nagel S. R., *Nature*, **396** (1998) 21.
[3] Corwin E. I., Jaeger H. M. and Nagel S. R., *Nature*, **435** (2005) 1075.
[4] Majmudar T. S. and Behringer R. P., *Nature*, **435** (2005) 1079; Ren J., Dijksman J. A. and Behringer R. P., *Phys. Rev. Lett.*, **110** (2013) 018302.
[5] Jaeger H. M., Liu C. and Nagel S. R., *Phys. Rev. Lett.*, **62** (1988) 1.
[6] Falcon E., Fauve S. and Laroche C., *Eur. Phys. J. B*, **9** (1999) 183.
[7] Falcon E., Aumaître S., Evesque P., Palencia F., Lecoutre-Chabot C., Fauve S., Beysens D. and Garrabos Y., *EPL*, **74** (2006) 830.
[8] Puglisi A., Loreto V., Marconi U. M. B., Petri A. and Vulpiani A., *Phys. Rev. Lett.*, **81** (1998) 3848; Losert W., Cooper D. G. W., Delour J., Kudrolli A. and Gollub J. P., *Chaos*, **9** (1999) 682; Olafsen J. S. and Urbach J. S., *Phys. Rev. E*, **60** (1999) R2468(R); Rouyer F. and Menon N., *Phys. Rev. Lett.*, **85** (2000) 3676; van Zon J. S., Kreft J., Goldman D. I., Miracle D., Swift J. B. and Swinney H. L., *Phys. Rev. E*, **70** (2004) 040301(R); Harth K., Kornek U., Trittel T., Strachauer U., Höme S., Will K. and Stannarius R., *Phys. Rev. Lett.*, **110** (2013) 144102; Scholz C. and Pöschel T., *Phys. Rev. Lett.*, **118** (2017) 198003.
[9] McNamara S., *Phys. Fluids*, **5** (1993) 3056; Goldhirsch I. and Zanetti G., *Phys. Rev. Lett.*, **70** (1993) 1619; Brilliantov N., Salueña C., Schwager T. and Pöschel T., *Phys. Rev. Lett.*, **93** (2004) 134301.
[10] McNamara S. and Young W. R., *Phys. Fluids A*, **4** (1992) 496.
[11] Haff P. K., *J. Fluid Mech.*, **134** (1983) 401.
[12] Maass C. C., Isert N., Maret G. and Aegerter C. M., *Phys. Rev. Lett.*, **100** (2008) 248001; Grasselli Y., Bossis G. and Goutallier G., *EPL*, **86** (2009) 60007; Tatsumi S., Murayama Y., Hayakawa H. and Sano M., *J. Fluid Mech.*, **641** (2009) 521; Harth K., Trittel T., Wegner S. and Stannarius R., *Phys. Rev. Lett.*, **120** (2018) 214301.
[13] Kudrolli A., Wolpert M. and Gollub J. P., *Phys. Rev. Lett.*, **78** (1997) 1383.
[14] Falcon E., Wunenburger R., Évesque P., Fauve S., Chabot C., Garrabos Y. and Beysens D., *Phys. Rev. Lett.*, **83** (1999) 440.
[15] Opsomer E., Ludewig F. and Vandewalle N., *Phys. Rev. E*, **84** (2011) 051306.
[16] See `https://spacegrains.org`.
[17] Aumaître S., Behringer R. P., Cazaubiel A., Clément E., Crassous J., Durian D. J., Falcon E., Fauve S., Fischer D., Garcimartín A., Garrabos Y., Hou M., Jia X., Lecoutre C., Luding S., Mazza D., Noirhomme M., Opsomer E., Palencia F., Pöschel T., Schockmel J., Schröter M., Sperl M., Stannarius R., Vandewalle N. and Yu P., *Rev. Sci. Instrum.*, **89** (2018) 075103.
[18] Opsomer E., Ludewig F. and Vandewalle N., *EPL*, **99** (2012) 40001.
[19] Bannerman M. N., Kollmer J. E., Sack A., Heckel M., Mueller P. and Pöschel T., *Phys. Rev. E*, **84** (2011) 011301; Sack A., Heckel M., Kollmer J. E., Zimber F. and Pöschel T., *Phys. Rev. Lett.*, **111** (2013) 018001; Kollmer J. E., Tupy M., Heckel M., Sack A. and Pöschel T., *Phys. Rev. Appl.*, **3** (2015) 024007.
[20] Opsomer E., PhD Thesis, Univ. Liège (2014).
[21] Kollmer J. E., Sack A., Heckel M. and Pöschel T., *New J. Phys.*, **15** (2013) 093023.
[22] Schindelin J., Arganda-Carreras I., Frise E., Kaynig V., Longair M., Pietzsch T., Preibisch S., Rueden C., Saalfeld S., Schmid B., Tinevez J.-Y., White D. J., Hartenstein V., Eliceiri K., Tomancak P. and Cardona A., *Nat. Methods*, **9** (2012) 676.
[23] Gilet T., Vandewalle N. and Dorbolo S., *Phys. Rev. E*, **79** (2009) 055201(R).
[24] O'Hern C. S., Langer S. A., Liu A. J. and Nagel S. R., *Phys. Rev. Lett.*, **88** (2002) 075507; Onoda G. Y. and Liniger E. G., *Phys. Rev. Lett.*, **64** (1990) 2727; Jerkins M., Schröter M., Swinney H. L., Senden T. J., Saadatfar M. and Aste T., *Phys. Rev. Lett.*, **101** (2008) 018301.